Parasitology International 85 (2021) 102435

Contents lists available at ScienceDirect

Parasitology International

journal homepage: www.elsevier.com/locate/parint

cAMP-dependent protein kinase regulates secretion of apical membrane antigen 1 (AMA1) in *Plasmodium yoelii*

Takahiro Ishizaki [a,b,c], Masahito Asada [a,b,d], Hassan Hakimi [b,e], Nattawat Chaiyawong [a,b], Yuto Kegawa [a,b,f], Kazuhide Yahata [b], Osamu Kaneko [a,b,*]

[a] Program for Nurturing Global Leaders in Tropical and Emerging Communicable Diseases, Graduate school of Biomedical Sciences, Nagasaki University, 1-12-4 Sakamoto, Nagasaki 852-8523, Japan
[b] Department of Protozoology, Institute of Tropical Medicine (NEKKEN), Nagasaki University, Nagasaki, 1-12-4 Sakamoto, Nagasaki 852-8523, Japan
[c] Laboratory for Molecular Infection Medicine Sweden, Department of Molecular Biology, Umeå University, Umeå 901 87, Sweden
[d] National Research Center for Protozoan Diseases, Obihiro University of Agriculture and Veterinary Medicine, Nishi 2-11, Obihiro, Hokkaido 080-0834, Japan
[e] Department of Veterinary Pathobiology, College of Veterinary Medicine, Texas A&M University, College station, TX 77843, USA
[f] Section on Integrative Biophysics, Eunice Kennedy Shriver National Institutes of Child Health and Human Development, National Institute of Health, 9000 Rockville Pike, Bethesda, Mary land 20892, USA

ARTICLE INFO

Keywords:
Plasmodium yoelii
DiCre
Inducible knockout
cAMP-dependent protein kinase
Rhoptry neck protein 2
Malaria

ABSTRACT

Malaria remains a heavy global burden on human health, and it is important to understand the molecular and cellular biology of the parasite to find targets for drug and vaccine development. The mouse malaria model is an essential tool to characterize the function of identified molecules; however, robust technologies for targeted gene deletions are still poorly developed for the widely used rodent malaria parasite, *Plasmodium yoelii*. To overcome this problem, we established a DiCre-loxP inducible knockout (iKO) system in *P. yoelii*, which showed more than 80% excision efficacy of the target locus and more than 90% reduction of locus transcripts 24 h (one cell cycle) after RAP administration. Using this developed system, cAMP-dependent protein kinase (PKAc) was inducibly disrupted and the phenotypes of the resulting PKAc-iKO parasites were analyzed. We found that PKAc-iKO parasites showed severe growth and erythrocyte invasion defects. We also found that disruption of PKAc impaired the secretion of AMA1 in *P. yoelii*, in contrast to a report showing no role of PKAc in AMA1 secretion in *P. falciparum*. This discrepancy may be related to the difference in the timing of AMA1 distribution to the merozoite surface, which occurs just after egress for *P. falciparum*, but after several minutes for *P. yoelii*. Secretions of PyEBL, Py235, and RON2 were not affected by the disruption of PKAc in *P. yoelii*. PyRON2 was already secreted to the merozoite surface immediately after merozoite egress, which is inconsistent with the current model that RON2 is injected into the erythrocyte cytosol. Further investigations are required to understand the role of RON2 exposed on the merozoite surface.

1. Introduction

Malaria is still a major public health concern in the world [1]. The causative pathogens of malaria are obligate intracellular protozoan parasites which belong to the genus *Plasmodium* and are transmitted by *Anopheles* mosquitoes. In humans, parasites proliferate in erythrocytes and the clinical symptoms are caused by these blood stage parasites. Because malaria parasites are obligate intracellular organisms, erythrocyte invasion is a critical step for their survival. Invasion is mediated by the sequential secretion of molecules from parasite organelles, including micronemes and rhoptries, which have unique roles such as interaction with erythrocyte receptors [2–4]. Secretion of these molecules is regulated by intracellular calcium mobilization and phosphorylation [5,6]. In *Plasmodium falciparum*, merozoite released from erythrocytes exposes them to the low potassium environment of the blood and triggers elevation of cytosolic calcium, which in turn stimulates AMA1 and EBA-175 secretion from micronemes. Recognition of erythrocyte surface glycophorin A by EBA-175 restores basal cytosolic

* Corresponding author at: Department of Protozoology, Institute of Tropical Medicine (NEKKEN), Nagasaki University, 1-12-4 Sakamoto, Nagasaki 852-8523, Japan.
E-mail addresses: masada@obihiro.ac.jp (M. Asada), hhakimi@obihiro.ac.jp (H. Hakimi), kyahata@nagasaki-u.ac.jp (K. Yahata), okaneko@nagasaki-u.ac.jp (O. Kaneko).

https://doi.org/10.1016/j.parint.2021.102435
Received 12 July 2021; Received in revised form 6 August 2021; Accepted 6 August 2021
Available online 11 August 2021

calcium levels and triggers secretion of rhoptry body protein Clag3.1 [2]. Signaling of AMA1 secretion is regulated by hierarchical phosphorylation by cyclic AMP (cAMP)-dependent protein kinase (PKA) and glycogen synthase kinase 3 (GSK3) [7,8]. cAMP is synthesized from ATP by adenylyl cyclase and works as a second messenger. Once the cellular cAMP concentration reaches a threshold level, PKA is activated and phosphorylates Ser_{610} of *P. falciparum* AMA1, which is essential for erythrocyte invasion [7,9–11]. This model was developed by analyzing *P. falciparum*, which can invade erythrocytes immediately after egress; however, other malaria parasite species such as *P. yoelii* and *P. knowlesi* require several minutes after egress for merozoites to achieve competency to invade erythrocytes, indicating that these parasites need to be activated after egress [12]. Understanding this activation process would provide insights to understand the erythrocyte invasion mechanisms of malaria parasites.

To utilize reverse genetics to describe the function of essential parasite proteins for erythrocyte invasion, technologies are required to inducibly knock down or knock out target molecules. To this end, we have recently established a tetracycline-repressive transactivator (Tet-off) system in *P. yoelii*, but this system requires a time-consuming optimization process to modify the 5′ untranslated region of the target gene [13]. In the present study we established a dimerisable Cre-recombinase (DiCre)-loxP inducible gene knockout system in *P. yoelii* by adapting methods developed for *P. falciparum* and *P. berghei* [14,15], and assessed the consequence of the disruption of PKAc in the erythrocyte invasion process of *P. yoelii*.

2. Materials and methods

2.1. Parasites and animal experiment

The *P. yoelii* 17XL strain was maintained in 6–8 week old female ICR or BALB/c mice (Japan SLC, Hamamatsu, Japan). Animal experiments were approved by the Animal Care and Use Committee of Nagasaki University (Permit number: 1403031120–5).

2.2. Plasmid construction and transfection

The plasmid pBS_DC_hsp86/Bip5' was a kind gift from M. Blackman [14]. The promoter to drive FRB-Cre60 and FKBP-Cre59 was replaced with the *P. yoelii* elongation factor 1 alpha (ef-1α) bi-directional promoter (pBS-DC-Pyef-1α). The DiCre expression cassette was PCR-amplified from pBS-DC-Pyef-1α using oligonucleotide primers DiCre.F and DiCre.R, and ligated into the pDC2-cam-Cas9-PyU6-hDHFR plasmid using an In-Fusion HD cloning kit (Takara Bio Inc., Shiga, Japan), yielding pDC2-Cas9-DC-Pyef-1α [16]. A guide RNA (gRNA) sequence to introduce a double strand break in the *p230p* locus (PY17X_0306600) was designed using EupaGDT and ligated using T4 ligase (New England Biolabs, Ipswich, MA, USA). The 5′- and 3′- homologous regions (HRs) were PCR-amplified from parasite gDNA with oligonucleotide primers Pyp230p 5HR.F, Pyp230p-5HR.R, Pyp230p-3HR.F, and Pyp230p-3HR.R; and inserted into pDC2-Cas9-DC-Pyef-1α, yielding pDC2-Cas9-p230p-DC-Pyef-1α.

The PKAc 5′- and 3'-HRs were PCR-amplified from parasite gDNA. A DNA fragment containing a loxP intron sequence [17] and recodonized PKAc cDNA sequence corresponding to exons 2 to 5 designed based on the codon usage of *P. falciparum* (3D7 strain) with the IDT codon optimization tool (https://sg.idtdna.com/CodonOpt; GenScript Biotech, Piscataway, New Jersey, USA) were synthesized. Recodonization was done to avoid unwanted integration to this region in the genome by homologous recombination, instead of the 5'-HR. A DNA fragment containing hDHFR-yFCU open reading frame was PCR-amplified from pDC2-Cas9-PyU6-PypPK1-myc plasmid with primers PKAc-iKOhDHFR/yFCU·F and PKAc-iKO-hDHFR/yFCU.R [16]. All PCR products were purified using a gel extraction kit and ligated into pDC2-Cas9-PyU6-hDHFR plasmid using an In-Fusion HD cloning kit, yielding pDC2-Cas9-PyU6-PKAc-iKO-hDHFR/yFCU. Transfection to *P. yoelii* was performed as described [13]. Drinking water containing 1 mg/mL 5-fluorocytosine (5-FC; Sigma-Aldrich, St. Louis, Missouri, USA) was orally administrated to mice infected with DiCre-expressing *P. yoelii* parasites to obtain parasites without the drug cassette, followed by cloning of transgenic parasites by limiting dilution [18]. The presence of the DiCre expression cassette and the loxP insertion sequences in the obtained parasites were verified by PCR-based genotyping using specific primer pairs (Table S1).

2.3. Southern blotting

Ten micrograms of gDNA extracted from DiCre-expressing parasites was double-digested with *Stu*I and *Eco*RI, or *Sac*I and *Kpn*I. Genomic DNA from PKAc-iKO parasites was double-digested with *Eco*RV and *Ale*I, or EcoRV and *Not*I. Digested gDNA was separated by agarose gel electrophoresis, then transferred onto a HyBond N+ membrane (GE Healthcare, Buckinghamshire, U.K.). Four probes were generated: probe 1 with primers (p230p-Probe1.F and p230p-Probe1.R) for the *p230p* sequence, probe 2 (Cre60-Probe2.F and Cre60-Probe2.R) for the *cre60* sequence, probe 3 (PKAc-Probe3.F and PKAc-Probe3.R) for the *-pkac* sequence, and probe 4 (hDHFR-Probe4.F and hDHFR-Probe4.R) for the *hdhfr* sequence. All probes were labeled and hybridized using an AlkPhos Direct kit (GE Healthcare) [19]. Chemiluminescent signal was developed with the CDP-star detection reagent (GE Healthcare) and detected with a multipurpose charge-coupled-device (CCD) camera system (Las-4000 mini EPUV; Fujifilm, Japan).

2.4. Rapamycin treatment and evaluation of DiCre-loxP recombination efficacy

Rapamycin (RAP; Sigma-Aldrich) was dissolved in DMSO (4 mg/mL) and stored at −20 °C until use [15]. Schizont stage parasites were enriched using Nycodenz (1.077 g/mL; company info) and incubated at 15 °C for 3 h until their maturation. Matured schizonts were intravenously inoculated into mice and 4 mg/kg RAP resuspended in PBS was intraperitoneally administrated. Blood was collected from 3 mice at 3, 6, 12, and 24 h after RAP administration. Parasite DNA was extracted using a QIAamp DNA blood mini kit (Qiagen, Hilden, Germany) and PCR and quantitative PCR (qPCR) were carried out to evaluate Cre-loxP recombination efficacy. Excision efficacy was estimated by values obtained by two independent qPCR amplifications with primers P7 and P8 for uncleaved events and primers P9 and P10 for cleaved events. Excision efficacies (%) were calculated by the following formula: 100 x (values with P9/P10 primer set) / (values with P7/P8 primer set) + (values with P9/P10 primer set).

2.5. RNA extraction, cDNA synthesis, and quantitative reverse-transcription polymerase chain reaction (qRT-PCR)

To examine mRNA reduction levels of the DiCre-loxP system, infected blood of PKAc-iKO parasites was collected from 3 mice at 3, 6, 12, and 24 h after RAP or DMSO administration. Parasite pellets were resuspended in TRIzol (Thermo Fisher Scientific, Waltham, MA, USA) and total RNA was extracted according to the manufacturer's instructions. Extracted RNA was treated with DNase I (Promega, Madison, WI, USA) and further purified using an SV Total RNA Isolation System (Promega) kit. Complementary DNA (cDNA) synthesis was carried out using SuperScript III (Invitrogen, Carlsbad, CA, USA) following the manufacturer's instructions. qRT-PCR was performed to quantitate transcripts of recodonized *pkac* and *met-trna synthetase* with Power SYBR™ Green PCR Master Mix (Thermo Fisher Scientific) and specific primer pairs (Table S1) using a 7500 Real-Time PCR system (Applied Biosystems, Foster City, CA, USA). Values for *pkac* transcripts were normalized to those for *met-trna synthetase* transcripts.

2.6. Western blotting

Western blot analysis was performed to evaluate the DiCre protein expression level and the efficacy of Cre excision of the loxP pair. Parasite-infected erythrocytes were collected at 24 and 48 h after RAP administration, treated with 0.1% saponin, and proteins were extracted with 1% Triton X-100 in PBS containing protease inhibitor cocktail (cOmplete™; Sigma-Aidrich). SDS-PAGE and Western blot were performed as described [16]. Membranes were probed for 1 h at room temperature (RT) with mouse anti-Cre monoclonal antibody (1:1000; 2D8; Sigma-Aldrich), rabbit anti-FKBP12 antibody (1:1000; ab2918; Abcam, Cambridge, UK), mouse anti-Myc monoclonal antibody (1:1000; 9B11; Cell Signaling Technology, Danvers, MA, USA), or rabbit anti-PyAMA1 polyclonal antibody (1:300) [20]. Secondary hybridization was with HRP-conjugated anti-mouse IgG or anti-rabbit IgG (1:12000; Promega) for 1 h at RT. Bands were detected as described [16]. The band intensities were quantified with ImageJ software [21].

2.7. Indirect immunofluorescent assay (IFA)

IFA analysis was performed to evaluate the expression of FRB-Cre60 and FKBP-Cre59 and the loss or the reduction of PKAc proteins. Thin blood smears on glass slides were prepared from infected mice at the same time points as samples collected for Western blot analysis. Smears were fixed with 4% paraformaldehyde and 0.075% glutaraldehyde (PFA-GTA) in PBS for 15 min at RT, permeabilized with 0.1% Triton X-100 in PBS for 10 min at RT, and further incubated in 3% BSA in PBS for 1 h at RT for blocking. Mouse anti-Cre monoclonal antibody (1:250), rabbit anti-FKBP12 polyclonal antibody (1:250), or mouse anti-Myc monoclonal antibody (1:500) were used as primary antibodies. Alexa fluor 488-conjugated goat anti-mouse IgG or Alexa fluor 594-conjugated goat anti-rabbit IgG were used as secondary antibodies (1:1000). Smears were incubated with primary antibody for 1 h at RT and incubated with secondary antibody and 4′,6-diamidino-2-phenylindole (DAPI) for 30 min at RT. IFA smears were mounted with antifade medium (VECTASHIELD; Vector laboratories, Burlingame, CA, USA) and images were acquired using a confocal microscope (A1R; Nikon, Tokyo, Japan) with a 60× N.A. 1.40 CFI Plan Apo VC oil-immersion objective lens (Nikon).

2.8. Monitoring parasitemia

PKAc-iKO parasites (10^6) were inoculated into three mice and RAP or DMSO was injected intraperitoneally when the parasitemias reached 1%. Thin blood smears were prepared every 6 h from 24 to 48 h after inoculation and stained with Giemsa solution. To evaluate parasitemia, at least 5000 erythrocytes or 500 parasite-infected erythrocytes were counted. Parasite stages were classified into ring, small late trophozoite, large late trophozoite, and schizont stages. Small *versus* large late trophozoites were distinguished based upon diameter; specifically, less than 50% of erythrocyte diameter *versus* equal to or more than 50%, respectively. Schizonts were defined as parasites with more than one nucleus. Statistical analysis was conducted using two-way ANOVA analysis and Tukey's multiple comparison test using GraphPad Prism 8 (GraphPad software Inc., San Diego, CA).

2.9. Invasion assay

To evaluate invasion efficacy, an *in vitro* invasion assay was performed as described [22]. Briefly, purified matured schizonts (10^8) were filtrated and released merozoites were mixed with erythrocytes and incubated for 18 h with a 5% O_2, 5% CO_2, and 90% N_2 gas mixture. Giemsa-stained thin blood smears were prepared, and 10,000 erythrocytes were counted to estimate parasitemia. Significant difference of the parasitemia was evaluated by one-way ANOVA followed by Dunnett multiple comparison test using GraphPad Prism 8.

2.10. Secretion assay

To evaluate protein secretion from organelles to the merozoite surface, a secretion assay was performed basically as described [16]. In brief, merozoites were filtrated at 15 °C and incubated for 0 or 10 min at 37 °C, then were fixed with PFA-GTA for 15 min and transferred onto poly-L-lysine-coated cover slips. Cover slips were incubated with 3% BSA in PBS for 1 h, then with primary antibodies for 1 h. Primary antibodies were washed away with PBS, and then the coverslips were incubated with secondary antibodies for 30 min. Primary antibodies were rabbit anti-PyAMA1 (1:250) [20], mouse anti-Py235 (1:250; mAb 25.87, a kind gift from A. Holder) [23], rabbit anti-PyRON2 (1:250) antibody [20], rabbit anti-PyEBL antibody (1:250) [24], mouse anti-RON4 monoclonal antibody (Ab48F8) (1:250; a kind gift from D. Narum) [25], mouse anti-RON5 antibody (1:250) [20], and mouse anti-RhopH2 monoclonal antibody (mAb#25) (1:250) [26]]. Chicken anti-MSP1 (1:500) antibody [20] was used to identify parasites and, when applicable, mouse anti-HSP70 antibody was used to verify that parasite membranes were intact. The Alexa fluor 488-conjugated goat anti-chicken IgY (1:1000), Alexa fluor 568-conjugated goat anti-mouse IgG (1:1000), and Alexa fluor 647-conjugated anti-rabbit IgG (1:1000) were used as secondary antibodies. IFA images were acquired using a confocal microscope (A1R; Nikon) using a 60× N.A. 1.27 CFI Plan Apo Lambda 60× oil-immersion objective lens (Nikon) under identical conditions for all assays. The "sum intensity" (a value obtained by summing up intensity values of all pixels) and "signal-positive area" were obtained using NIS-elements software (Nikon). IFA images were also captured by super-resolution structured illumination microscopy (SR-SIM; LSM780/ERYRA PS1; Zeiss, Germany) using a 100× N.A. 1.46 alpha Plan-Apochromat oil-immersion objective (Zeiss), and EM-CCD camera iXon DU885 (Andor, UK). SR-SIM images were processed using ZEN software (Zeiss).

2.11. Time lapse analysis

Time-lapse analysis was conducted as described [13]. RAP or DMSO was administrated to mice infected with PKAc-iKO parasites and 24 h later matured schizonts were enriched using Nycodenz as described above. Merozoites were obtained from matured schizonts by filtration and kept at 15 °C. Mouse erythrocytes were applied to μ-slide VI 0.4 chambers (ibidi, Germany) and then purified merozoites were transferred into the slide chamber. Video images were captured at 2 fps for up to 40 min using a CCD camera (ORCA-R2; Hamamatsu Photonics, Japan) at 37 °C under a temperature controller system (Tokai Hit, Japan). Obtained video images were converted to AVI format using NIS-Element software (Nikon). A merozoite was judged as "non-detachment" if it did not invade and did not detach from an erythrocyte greater than or equal to 300 s after an erythrocyte deformation event. The frequency of each invasion event was statistically analyzed with Fisher's exact test using GraphPad Prism 8.

3. Results

3.1. Generation of a P. yoelii line constitutively expressing DiCre

To generate DiCre-expressing *P. yoelii*, a DNA fragment containing a DiCre expression cassette and a hDHFR-yFCU expression cassette was integrated into the *Pyp230p* gene locus, which is dispensable in all development stages [27] (Fig. 1A). After validating the insertion of this DNA fragment into the target genome locus by genotype PCR, parasites were treated with 5-FC to remove the hDHFR-yFCU expression cassette, then cloned by limiting dilution. Modification of the target gene locus was verified by genotype PCR and Southern blot analysis for all cloned parasite lines (Fig. 1B and C). Western blot analysis with an anti-Cre antibody that recognizes FRB-fused Cre60 (FRB-Cre60) or anti-FKBP12 antibody that recognizes FKBP12-fused Cre59 (FKBP-Cre59) revealed

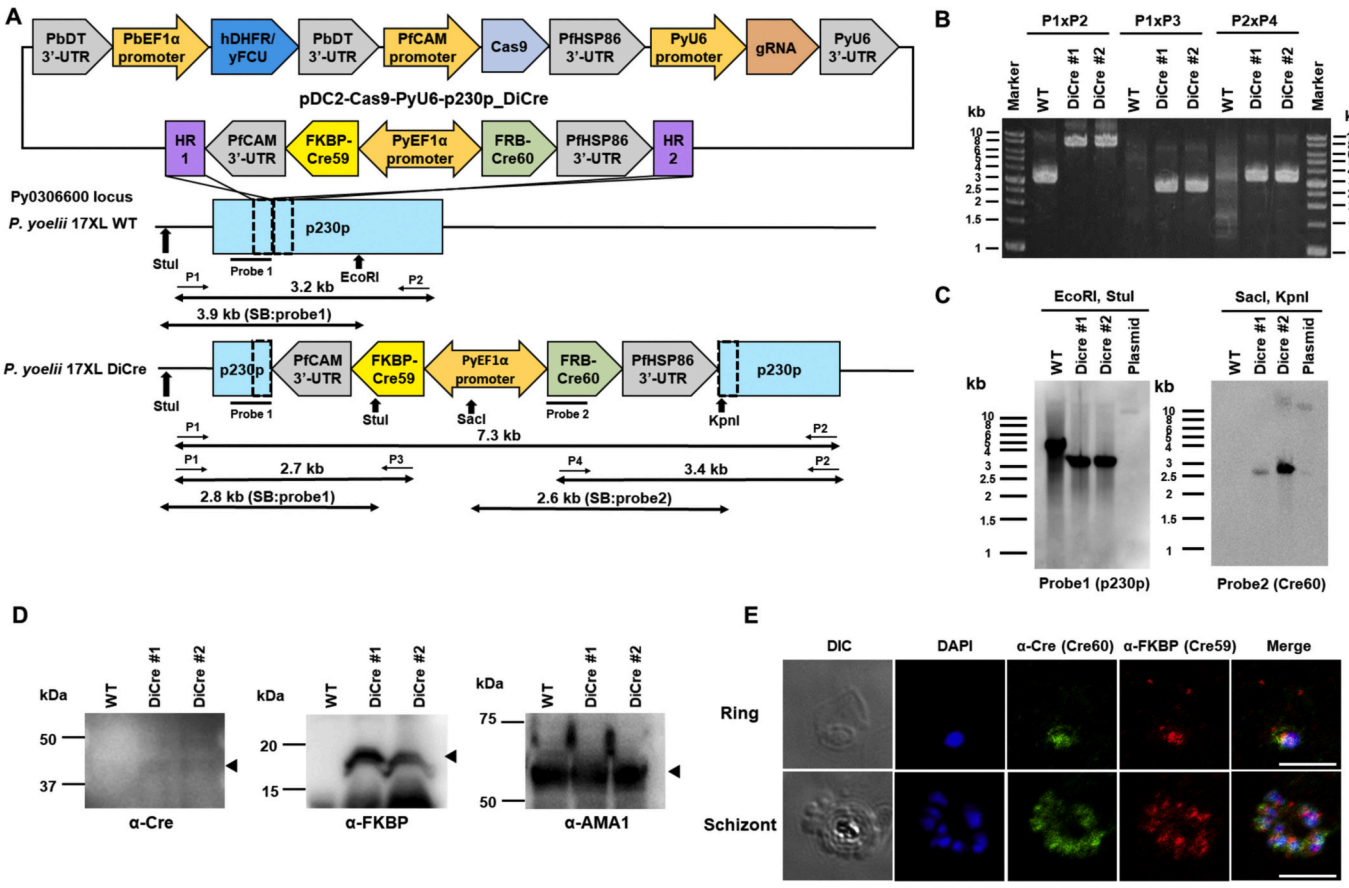

Fig. 1. Generation of DiCre-expressing parasites.
(A) Schematic of plasmid pDC2-Cas9-PyU6-p230p_DiCre, to generate DiCre expressing parasites. The DiCre expression cassette was designed to be integrated into the *P. yoelii p230p* (PY17X_0306600) gene locus. FRB-fused Cre60 (FRB-Cre60) and FKBP12-fused Cre59 (FKBP-Cre59) were driven by the bi-directional *P. yoelii* EF-1α promoter. (B) Genotyping PCR to evaluate the modification of the *p230p* gene locus. Expected band sizes are 3.2 kb in the parental wild type (WT) and 7.3 kb in DiCre (#1 and #2) parasites with primers P1 and P2 (P1xP2), no band in WT and 2.7 kb in DiCre parasites with primers P1 and P3 (P1xP3), and no band in WT and 3.4 kb in DiCre parasites with primers P2 and P4 (P2xP4). (C) Southern blot analysis to confirm the integration of the DiCre expression cassette. Probe 1 detected a 3.9-kb band in WT and a 2.8-kb band in cloned DiCre (#1 and #2) parasites. Probe 2 detected a 2.6-kb band in cloned DiCre parasites. The pDC2-Cas9-PyU6-p230p_DiCre plasmid digested with *Kpn*I was used as a control with an expected size of 13 kb. (D) Western blot analysis to confirm FRB-Cre60 and FKBP-Cre59 expression. Purified schizont proteins were extracted with Triton X-100 and reacted with anti-Cre, anti-FKBP12, or anti-PyAMA1 antibodies. Bands were detected around 45.1 kDa and 19.1 kDa for FRB-Cre60 and FKBP-Cre59, respectively. PyAMA1 was used as a loading control. (E) Dual IFA of ring and schizont stage DiCre parasites for FRB-Cre60 and FKBP-Cre59. Fluorescent signals with anti-Cre antibody (green), anti-FKBP12 (red), and DAPI nucleus signals (blue) were merged with differential interference contrast (DIC) images. Scale bar: 5 μm. (For interpretation of the references to colour in this figure legend, the reader is referred to the web version of this article.)

single bands at around 45 kDa or 19 kDa, respectively, consistent with the estimated molecular weight of these proteins (Fig. 1D). Protein extracts from wild type parasites did not show these bands, excluding potential non-specific reactions of anti-Cre or anti-FKBP12 antibodies. Western blot analysis with anti-AMA1 antibody ensured that the loaded protein amounts were similar (Fig. 1D bottom). IFA confirmed expression of FRB-Cre60 and FKBP-Cre59 at both the ring and schizont stages of DiCre-expressing *P. yoelii* clones, which largely colocalized with the nucleus signal (Fig. 1E). qRT-PCR revealed that the amount of *cre60* transcripts normalized by those of *met-trna synthetase* was not reduced for 29 days (9 passages in mice), indicating stable *cre60* transcription in the generated clone for at least one month (Fig. S1). Thus, we successfully generated *P. yoelii* clones constitutively expressing FRB-Cre60 and FKBP-Cre59 from their genome.

3.2. Generation of *P. yoelii* lines in which the PKAc gene locus can be inducibly disrupted

To further validate the developed DiCre system, we generated *P. yoelii* PKAc-iKO clones in which the PKAc gene locus can be inducibly disrupted by RAP administration (Fig. 2A). Modification and induced deletion of the PKAc gene locus was confirmed by PCR and Southern blot analysis (Fig. 2B and C). A clear positive 4.1 kb band was amplified by PCR with primers specific for the excised PKAc gene locus 24 h after RAP administration, but a faint 4.1 kb band was also observed before the addition of RAP in PKAc-iKO parasites, suggesting excision due to leaky expression of DiCre proteins without RAP. To examine the efficacy and timing of excision of the target region and the occurrence of undesired excision without RAP, qPCR and qRT-PCR were performed for samples collected at 0, 3, 6, 12, and 24 h after RAP or DMSO administration. The excision efficacy in PKAc-iKO clones #1 and #2 were 38 ± 2% and 36 ± 3% at 3 h after RAP administration, respectively, which reached 86 ± 3% and 85 ± 3% at 24 h after RAP administration, respectively. Meanwhile, excision was observed in PKAc-iKO clones #1 and #2 with DMSO at 24 h at rates of 10 ± 5% and 11 ± 1%, respectively (Fig. 2D). The estimated amount of *pkac* transcripts in PKAc-iKO #1 and #2 were reduced to 8 ± 0.0% and 3 ± 0.2% at 24 h after RAP administration, respectively (Fig. 2E). In addition, Western blot analysis of PKAc-iKO clones with anti-Myc antibody revealed a band around 43 kDa, consistent with the expected molecular weight of the PKAc protein, 43.8 kDa, before RAP administration (Fig. 2F NI). Normalized band intensities of samples with RAP treatment were much lower than those with DMSO

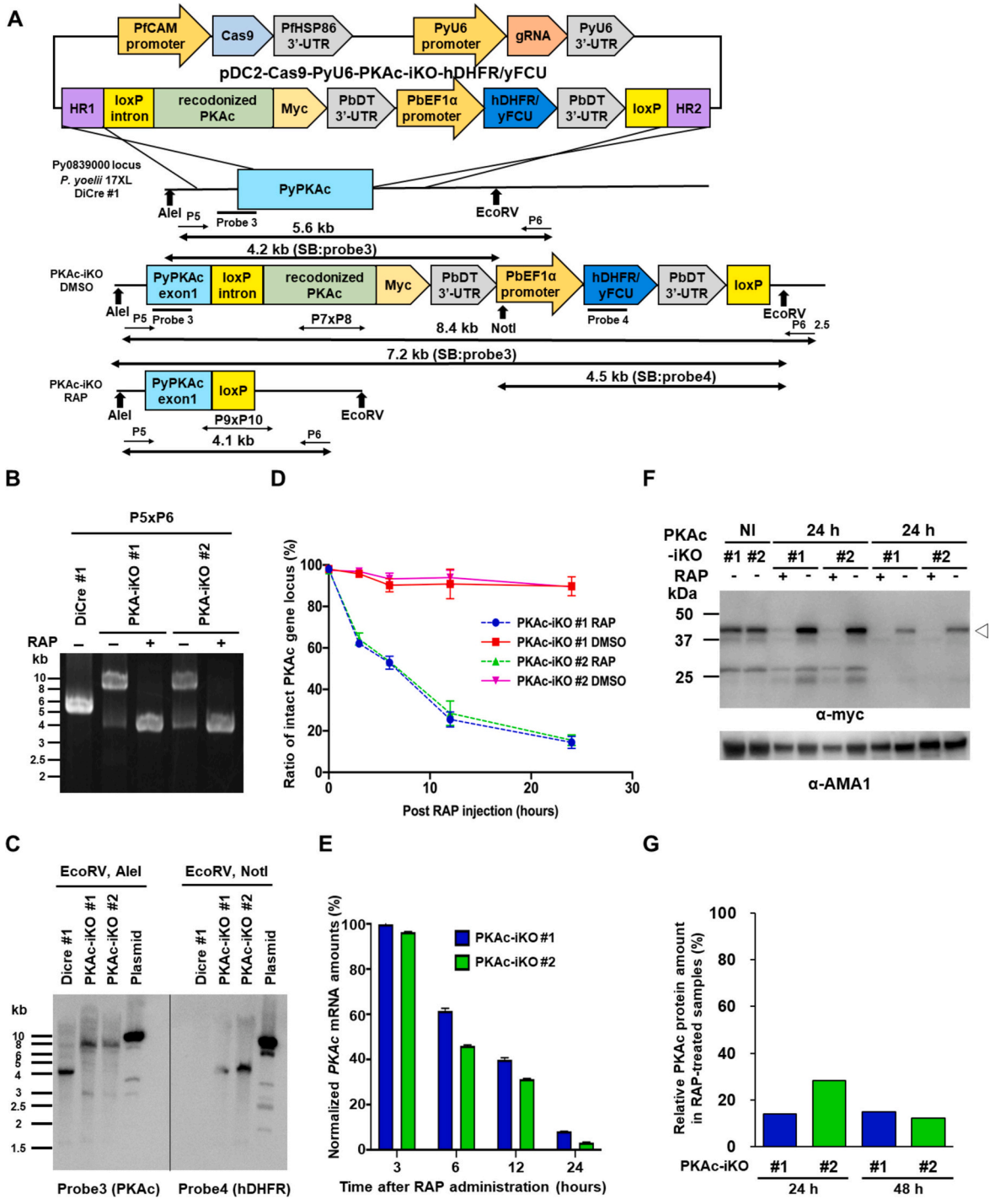

Fig. 2. Evaluation of DiCre-loxP recombination efficacy.
(A) Schematic of the plasmid to generate PKAc-iKO parasites (pDC2-Cas9-PyU6-PKAc-iKO-hDHFR/yFCU). An artificial loxP-intron was inserted between PKAc exon 1 and 2 in DiCre-expressing parasites. The sequence of exon 2 to exon 5 encoding PKAc was recodonized. Another loxP sequence was inserted between the hDHFR-yFCU expression cassette and the 3′ homology arm (HR2). (B) Genotyping PCR to evaluate the insertion and the excision of the DNA fragment in the PKAc gene locus. The expected PCR band size is 5.6 kb in WT and 8.2 kb in transgenic parasites after the insertion of CRISPR editing. The expected band size after the excision of the floxed region by RAP treatment is 4.1 kb. The gDNA was extracted from parasites 24 h after RAP or DMSO administration. (C) Southern blot analysis to confirm the modification of the PyPKAc gene locus. Probe 3 detected a 4.2 kb band in the parental DiCre parasite (#1) and a 7.2 kb band in the cloned PKAc-iKO parasites (#1 and #2). Probe 4 detected a 4.5 kb band in cloned PKAc-iKO parasites. pDC2-Cas9-PyU6-PKAc-iKO-hDHFR/yFCU plasmid digested with *Eco*RV was used as a control and the expected band size was 9.4 kb. (D) Ratio of intact PKAc gene locus. The proportion of the intact PKAc gene locus was estimated by qPCR at 0, 3, 6, 12, and 24 h after RAP or DMSO administration. (E) Relative amounts of PKAc transcripts were estimated by qRT-PCR at 0, 3, 6, 12, and 24 h after RAP or DMSO administration. (F) Western blot analysis to evaluate the relative amount of PKAc protein after RAP administration. An approximately 43 kDa band was detected with anti-Myc antibody. AMA1 served as a loading control. (G) The band intensities of PKAc in panel F were normalized with those of AMA1.

treatment at 24 h (14% and 28% for clones #1 and #2, respectively) and 48 h (15% and 12% for clones #1 and #2, respectively) after RAP administration (Fig. 2F and G).

3.3. PyPKAc is required to invade erythrocytes

Because the PKAc gene locus has been inducibly knocked out in *P. falciparum* [11], we compared the reported phenotype with *P. yoelii*. Firstly, we found that the growth of PKAc-iKO parasites treated with RAP was significantly lower than those treated with DMSO (Fig. 3A), consistent with the observation in *P. falciparum*. The parasitemias of wild type 17XL and cloned DiCre parasites with RAP treatment were not significantly different among all groups, indicating that RAP treatment had no effect on parasite growth (Fig. S2). Secondly, parasite stages affected by the excision of the PKAc gene locus were evaluated by comparing the proportion of the four asexual intraerythrocytic stages: early trophozoite (ring), small and late trophozoite, and schizont. The proportion of the ring stage was significantly reduced in both PKAc-iKO clones at 24 to 48 h after RAP treatment (Fig. 3B and Fig. S3), suggesting that PKAc had a role in parasite egress from or invasion into erythrocytes. Erythrocyte invasion assays performed *in vitro* with purified merozoites of PKAc-iKO clones revealed that invaded parasites with RAP treatment (0.04% and 0.06% for #1 and #2, respectively) were significantly lower than those treated with DMSO (0.8% and 0.9% for #1 and #2, respectively) (Fig. 3C). These data indicate that PKAc plays a role during erythrocyte invasion by *P. yoelii*, again consistent with the observation in *P. falciparum*.

3.4. AMA1 secretion was significantly reduced by disrupting PKAc in P. yoelii

Because secretion of the parasite ligands from the micro-organelles is essential for successful erythrocyte invasion, we investigated the effect of the disruption of PKAc on the secretion of several invasion-related organelle molecules. Firstly, we examined a microneme protein AMA1, whose cytoplasmic region was reported to be phosphorylated by PKAc in *P. falciparum* [11,28]. We found that AMA1 was detectable on the apical end of the merozoites purified at 15 °C. In *P. falciparum*, secretion of AMA1 is proposed to be triggered by egress and AMA1 is immediately distributed to the entire merozoite [29]. Analysis of DMSO-treated merozoites showed that the AMA1 signal-positive area was significantly increased after 10 min incubation, indicating that *P. yoelii* AMA1 was distributed from the apical end to the entire surface during that time span (Fig. 4C). The *P. yoelii* merozoite changes its shape from elongated to spherical after egress from the infected erythrocyte and prior to invasion [12]. Super-resolution microscopy visualized that the spread of AMA1 on the merozoite surface coincided with this morphological change of the merozoite (Fig. S4). Just after purification and after 10 min incubation at 37 °C, the sum intensity and the positive area of the merozoite surface AMA1 signal was significantly reduced by disrupting the PKAc gene locus with RAP treatment in comparison with the DMSO control (Fig. 4A-C). This result indicated that AMA1 secretion was impaired without PKAc in *P. yoelii*, in contrast to the report that AMA1 secretion in *P. falciparum* was not affected by disrupting PKAc [11].

3.5. RON2 is secreted onto the entire merozoite surface before attachment to the erythrocyte

We evaluated the effects of PKAc disruption on the secretion of another molecule, rhoptry neck protein 2 (RON2). RON2 is proposed to be injected into the invading erythrocyte and inserted into the erythrocyte membrane from the erythrocyte cytosol, to then make a complex with AMA1 to form a moving junction which serves as a scaffold for merozoite invasion. We found that RON2 was readily detectable on the entire merozoite surface just after purification, a time at which merozoites showed an elongated shape (Fig. 4D and S4). Following PKAc disruption, the sum intensity and signal-positive area of RON2 were not significantly different than in the presence of PKAc (Fig. 4E and F), indicating that RON2 secretion is independent of PKA and AMA1 secretion.

We examined additional *P. yoelii* invasion ligands EBL and Py235 (a homolog of *P. falciparum* reticulocyte binding protein like (RBL) proteins). PyEBL was detectable on the merozoite surface after 10 min incubation (Fig. 5A) as described [13] and Py235 was detected on the merozoite surface just after merozoite purification (Fig. 5D). Their secretion pattern did not change by PKAc disruption (Fig. 5B and C for PyEBL and 5E and 5F for Py235), indicating that secretion of EBL and Py235 are independent of PKAc and AMA1 secretion. We sought to examine the secretion of other rhoptry proteins, RON4, RON5, and RhopH2, but they were not detectable on the surface of the purified merozoite even after 10 min incubation at 37 °C (Fig. S5).

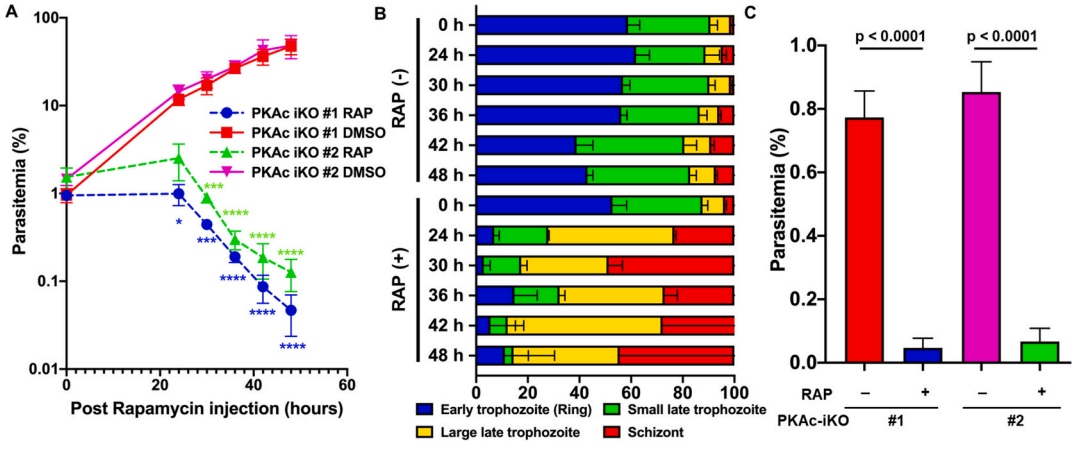

Fig. 3. *P. yoelii* PKAc is involved in erythrocyte invasion.
(A) Parasitemias were monitored at 0, 24, 30, 36, 42, and 48 h after RAP or DMSO administration for PKAc-iKO clones #1 and #2. Parasitemias of the RAP group significantly lower than that of the DMSO group are indicated with asterisks (*, $p < 0.05$; ***, $p < 0.001$; ****, $p < 0.0001$ by two-way ANOVA post-hoc Tukey's multiple comparison test). (B) The proportion of early trophozoite (ring), small late trophozoite, large late trophozoite, and schizont stages at 0, 24, 30, 36, 42, and 48 h after RAP administration were evaluated for PKAc-iKO #1 parasites. (C) *In vitro* erythrocyte invasion assay. The invasion efficacy of PKAc-iKO #1 and #2 parasites treated with RAP was significantly lower than those treated with DMSO (Tukey's multiple comparison test).

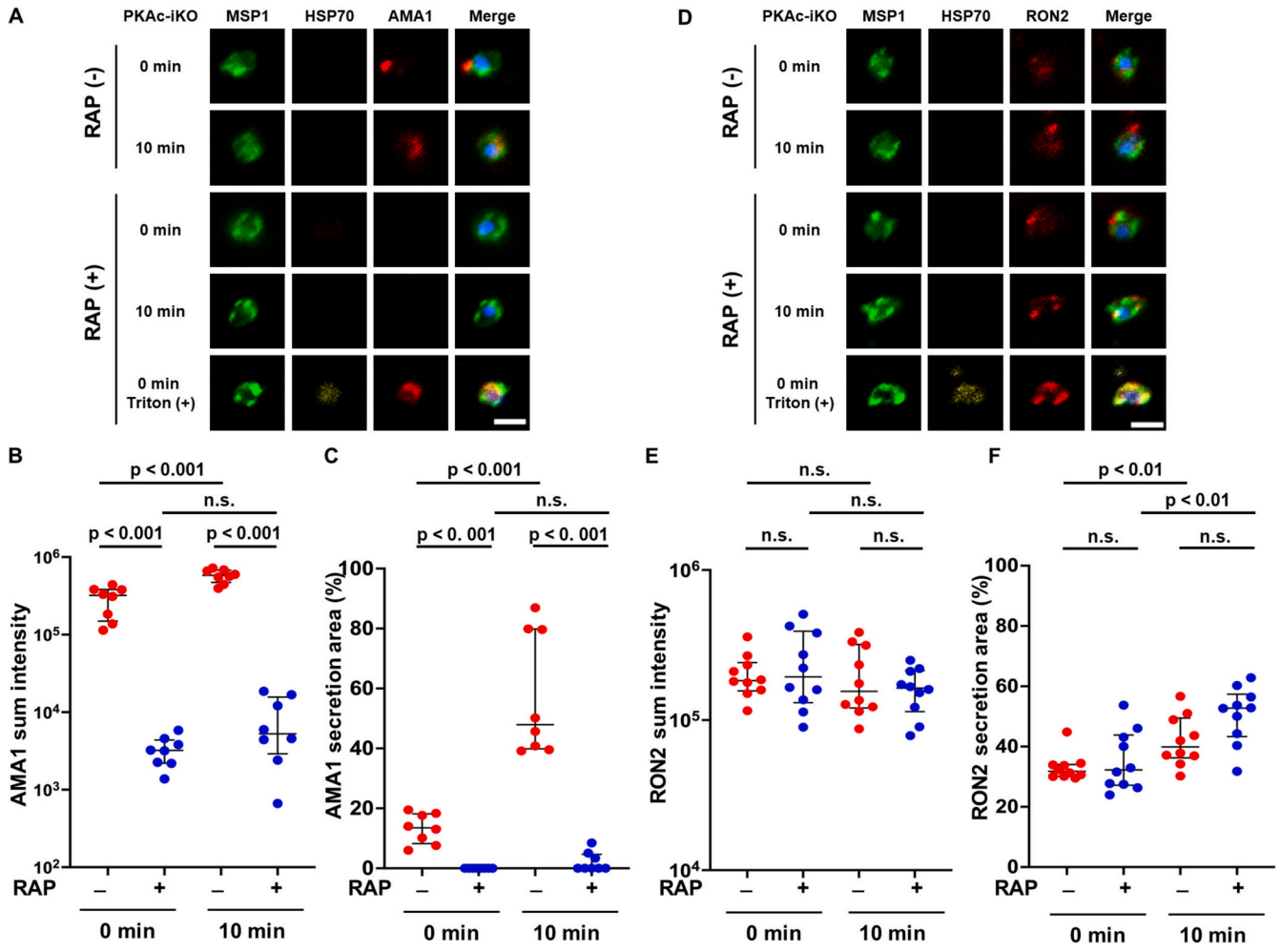

Fig. 4. PyPKAc regulates PyAMA1 secretion but not PyRON2 secretion.
(A) AMA1 secretion assay for PKAc-iKO parasites with or without rapamycin (RAP). (B) Sum intensity and (C) signal-positive area of AMA1 in PKAc-iKO parasites. (D) RON2 secretion assay for PKAc-iKO parasites with or without RAP. (E) Sum intensity and (F) signal-positive area of RON2 in PKAc-iKO parasites. Merozoite surface protein 1 (MSP1, green), heat shock protein 70 (HSP70, yellow), and AMA1 or RON2 (red). All images were merged with DAPI nucleus signals. RAP administration status is indicated as with (+) or without (−). Parasites were not treated with Triton X-100 unless indicated as (+). Scale bar is 2 μm. Sum intensity and signal-positive area (AMA1 or RON2 signal-positive area divided by MSP1 signal-positive area) were calculated with NIS-elements software. Differences were examined by pair-wise Mann-Whitney *U* test and $p < 0.01$ was taken as a significant difference. (For interpretation of the references to colour in this figure legend, the reader is referred to the web version of this article.)

3.6. Merozoites without PKAc were not able to complete the invasion process and were arrested on the erythrocyte surface

To determine the invasion steps inhibited by disrupting PKAc in *P. yoelii*, RAP- or DMSO-pretreated purified merozoites were mixed with fresh mouse erythrocytes and invasion events were recorded for 40 min for analysis as described [13]. We observed more than 60 merozoites attached to the erythrocyte for all experimental groups. Representative images and videos are provided (Fig. 6A selected from Video 1 and Video 2). The number of erythrocyte deformation events per number of merozoite attachment events in RAP-treated groups was 65% and 67% for clones #1 and #2, respectively, which were not significantly different from those in DMSO-treated groups (80% and 68% for clones #1 and #2 left panel) (Fig. 6B). This result indicated that disruption of PKAc did not affect merozoite initial attachment to the erythrocyte and the merozoite motor machinery, because erythrocyte deformation is thought to be caused by merozoite gliding motility [30]. The number of echinocytosis events per number of erythrocyte deformation events in RAP-treated groups were 0% and 2.1% for clones #1 and #2, respectively, which were significantly lower than those in DMSO-treated groups (20% and 37% for clones #1 and #2, respectively) ($p < 0.001$; Fig. 6B middle panel), indicating that disruption of PKAc had a significant negative impact on merozoite internalization into the erythrocyte. The number of merozoite detachment events from the erythrocyte per number of erythrocyte deformation events in RAP-treated groups was 28% and 27% for clones #1 and #2, respectively, which were not significantly different from those in DMSO-treated groups (29% and 26% for clones #1 and #2, respectively) (Fig. 6B right panel), indicating that even following PKAc disruption the tight junction between the invading merozoite and erythrocyte was formed. This phenotype is consistent with the observation in *P. falciparum* [11].

4. Discussion

Functional genomics, including targeted gene disruption methodologies, is important to identify targets of drug and vaccine development. For *Plasmodium*, gene disruption is facilitated by the haploid genome of the parasite but hindered by the fact that most knockout methods require genetic manipulation of asexual stage parasites. Asexual stage parasites express 45% of all parasite-encoded molecules, and many are difficult to disrupt and characterize due to their essentiality in this stage. To overcome this problem, inducible molecular genetics approaches, for

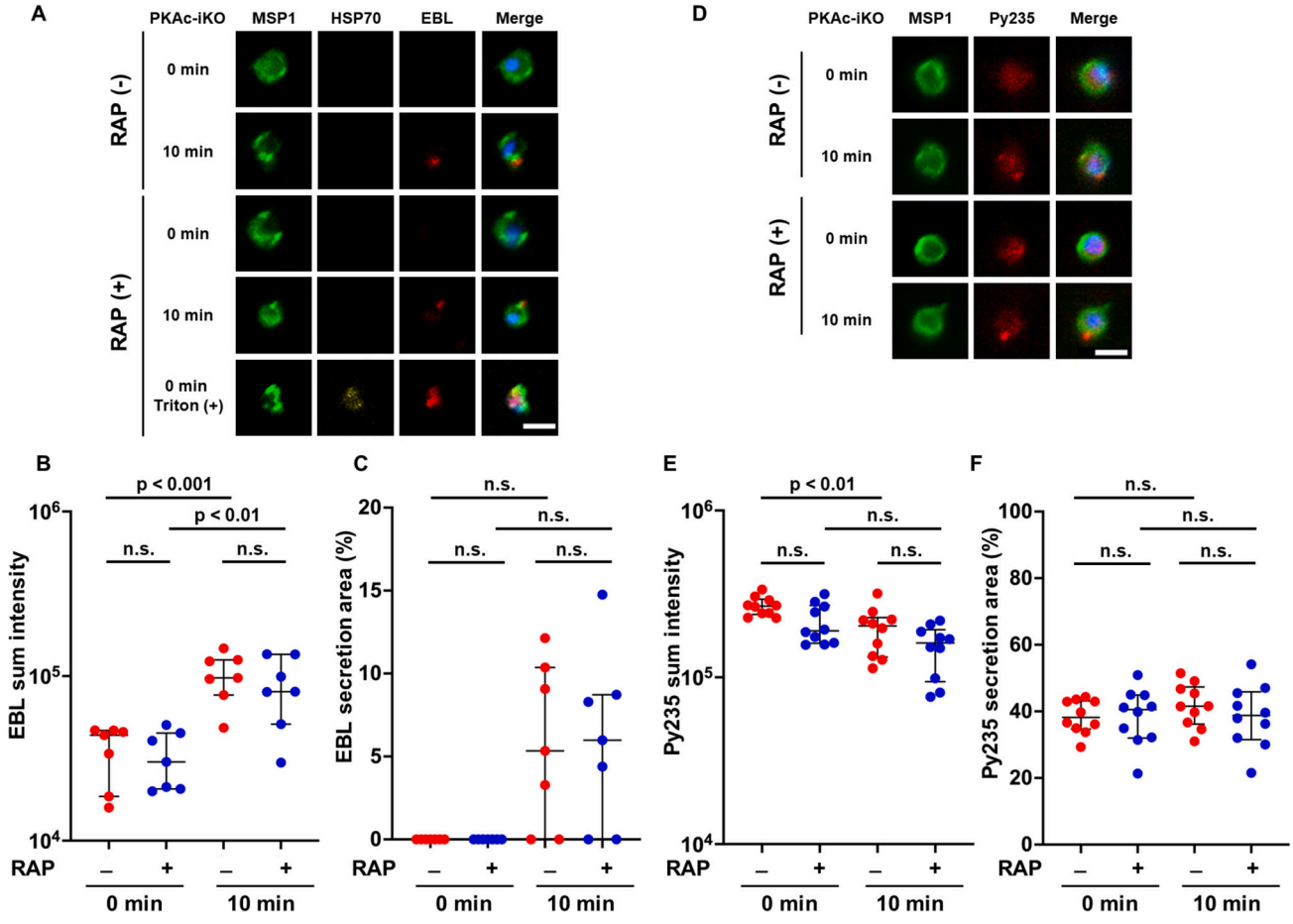

Fig. 5. Disruption of PyPKAc did not alter the secretion pattern of PyEBL and Py235.
(A) PyEBL secretion assay for PKAc-iKO parasites with or without rapamycin (RAP). (B) Sum intensity and (C) signal-positive area of PyEBL in PKAc-iKO parasites. (D) Py235 secretion assay for PKAc-iKO parasites with or without RAP. (E) Sum intensity and (F) signal-positive area of Py235 in PKAc-iKO parasites. EBL and Py235 signals are shown as red and other information is as described in Fig. 4. Scale bar is 2 μm. (For interpretation of the references to colour in this figure legend, the reader is referred to the web version of this article.)

instance transcriptional knockdown using the Tet on/off system, were developed in rodent malaria parasites [13,31]. However, the Tet on/off system approach requires a time-consuming optimization process for each modification. Thus, in the present study the DiCre-loxP inducible gene knockout system, which utilizes dimerization of FRB-Cre60 and FKBP-Cre59 with RAP for activation, was applied to *P. yoelii* based on the system developed in *P. falciparum* and *P. berghei* [14,15]. In our developed system in *P. yoelii* more than 80% excision efficacy of the target locus and more than 90% reduction of the transcripts 24 h (one cycle) after RAP administration were observed, consistent with the reports for *P. falciparum* and *P. berghei*, which showed recombination efficacy with more than 80% in one cycle (48 or 24 h, respectively) [15,17]. Indeed, we were able to observe an apparent phenotype on protein secretion from PKAc-iKO merozoites with RAP administration, indicating the usefulness of the developed system in *P. yoelii*.

We found that AMA1 secretion was impaired without PKAc in *P. yoelii*, in contrast to a report that *P. falciparum* was able to secret AMA1 normally following PKAc disruption [11]. One explanation is that phosphorylation of the AMA1 cytoplasmic region is required for the secretion of this molecule in *P. yoelii*, but not in *P. falciparum*. We reported that *P. yoelii* cannot invade erythrocytes immediately after egress, whereas *P. falciparum* was readily invasive at this timepoint [12]; although the underlying molecular mechanism for this observation is unclear. In this study, we found that the timing of AMA1 distribution on the merozoite surface is different between *P. yoelii* and *P. falciparum*; specifically, in *P. yoelii* AMA1 was not distributed to the merozoite surface for several minutes after release from the erythrocyte, whereas it is detectable over a large surface area of matured *P. falciparum* merozoites just after egress. It is of interest to explore if these differences in AMA1 behavior are related to the difference in the invasion phenotype between the two *Plasmodium* species.

Following PKAc disruption in *P. falciparum*, Patel et al. (2019) found that shedding of *P. falciparum* AMA1 was impaired and raised the possibility that the loss of interaction of unphosphorylated AMA1 and RON2 resulted in a failure of erythrocyte invasion [11]. This conclusion was based in part on a similar invasion inhibitory phenotype observed when the AMA1-RON2 interaction is inhibited by a peptide termed R1 [32,33]. In this study we observed that when PKAc is knocked out, the *P. yoelii* parasite was not able to secret AMA1 efficiently and its interaction with RON2 is expected to be reduced - thus AMA1 is directly involved in the reduced invasion phenotype in *P. yoelii*. It is plausible that other mechanisms that require PKA-dependent phosphorylation are also impaired in *P. yoelii* and participate in the reduced erythrocyte invasion activity, as proposed for *P. falciparum* [11].

Signal for RON2, but not RON4 and RON5, was detected on the merozoite surface just after purification in *P. yoelii*. The surface location of RON2 seems to be incompatible with the currently proposed role of RON2 in apicomplexan parasites; specifically, that a part of RON2 is exposed on the erythrocyte membrane, which is inserted from the erythrocyte cytosol, and interacts with AMA1 to form a moving junction [34–36]. RON2 located on the merozoite surface is unlikely to be injected into the erythrocyte cytosol. It is possible that a portion of

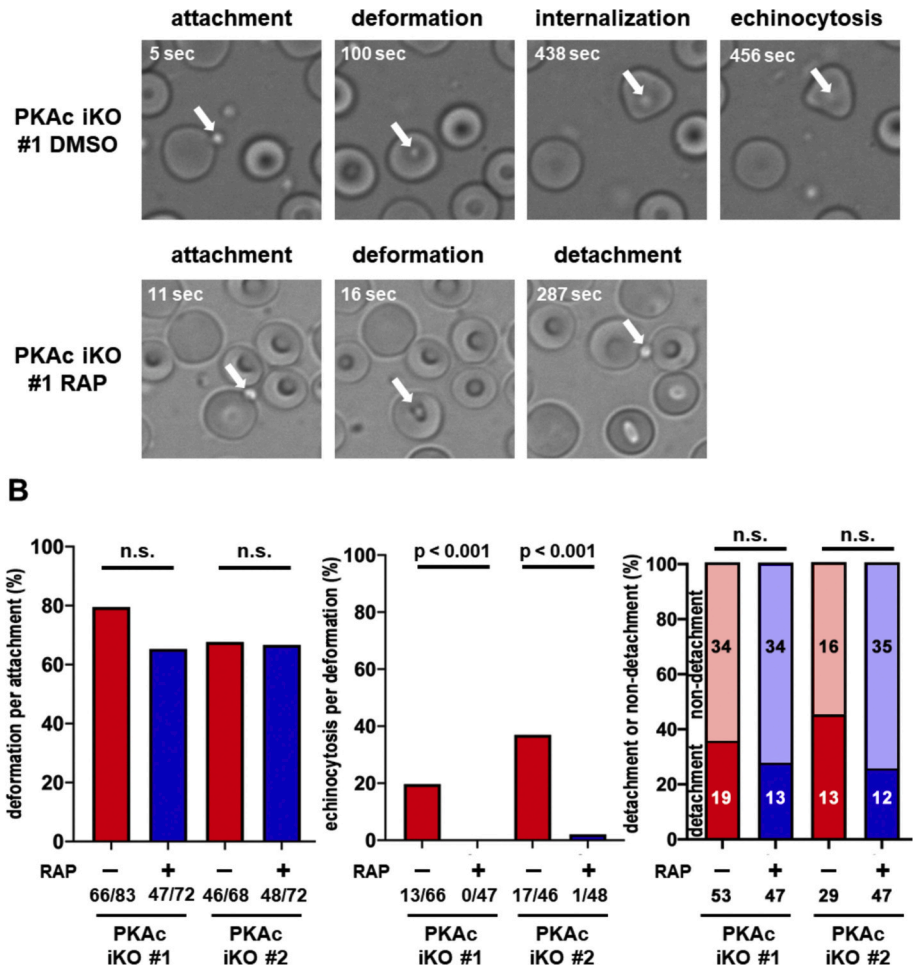

Fig. 6. Time-lapse imaging of erythrocyte invasion by PyPKAc-iKO parasites.
(A) Representative cropped images for each invasion step of PyPKAc-iKO parasites from time-lapse videos. Merozoite attachment, erythrocyte deformation, merozoite internalization, echinocytosis, and a non-detached merozoite are shown for the PKAc-iKO parasite clone #1 treated with RAP or DMSO. Arrows indicate merozoites. (B) The ratio of the number of erythrocyte deformations per the number of merozoite attachments (left) and the number of echinocytosis events per the number of erythrocyte deformations (middle) are shown. The ratio of the number of detachment or non-detached merozoites per the number of parasites attached but not causing erythrocyte deformation are shown. Observed event numbers in PKAc-iKO clones #1 and #2 treated with RAP (+) or DMSO (−) are shown on the bottom. Significance was evaluated by a two-tailed Fisher's exact test. n.s. indicates $p > 0.05$.

RON2 remains in the rhoptry neck and is injected into the erythrocyte cytosol to function as proposed. Any role of RON2 secreted to the merozoite surface just after the egress remains to be elucidated.

In conclusion, we established a DiCre-loxP-based inducible knock out system in *P. yoelii* and applied the system to evaluate PyPKAc functions. We found that disruption of PKAc impaired parasite growth; inhibited erythrocyte invasion; and diminished the secretion of AMA1, in contrast to a report in *P. falciparum* showing no role of PKAc in AMA1 secretion. We found that PyRON2 was secreted to the merozoite surface just after purification, which complicates the current model that RON2 is injected into the erythrocyte cytosol. This finding needs further investigation to understand the role, if any, of RON2 exposed on the merozoite surface.

Supplementary data to this article can be found online at https://doi.org/10.1016/j.parint.2021.102435.

Declaration of interests

None.

Acknowledgements

We thank M. Blackman for the pBS_DC_hsp86/Bip5' plasmid, J. Sattabongkot for the anti-PbHSP70 antibody, A. Holder for the anti-Py235 antibody, D. Narum for the anti-RON4 antibody, and T.J. Templeton for critical reading of the manuscript. This study was conducted at the Joint Usage/Research Center on Tropical Disease, Institute of Tropical Medicine (NEKKEN), Nagasaki University, Japan. TI is a recipient of DC1 scholarship from the Japan Society for the Promotion of Science (JSPS). NC and YK were supported by the leading program, Nagasaki University, Japan. This study was partly supported by grants from JSPS-KAKENHI (19H03461 to OK and 17J09408 to TI) and the Japan Science Society (Sasakawa Scientific Research Grant 2020-4042 to TI). The funders had no role in the study design, data collection and analysis, decision to publish, or manuscript preparation.

References

[1] World Health Organization, World Malaria Report 2020, World Health Organization, Geneva, 2020 (ISBN: 978-92-4-001579-1).
[2] S. Singh, M.M. Alam, I. Pal-Bhowmick, J.A. Brzostowski, C.E. Chitnis, Distinct external signals trigger sequential release of apical organelles during erythrocyte invasion by malaria parasites, PLoS Pathog. 6 (2) (2010), e1000764, https://doi.org/10.1371/journal.ppat.1000764.
[3] G.E. Weiss, P.R. Gilson, T. Taechalertpaisarn, W.-H. Tham, N.W.M. de Jong, K. L. Harvey, F.J.I. Fowkes, P.N. Barlow, J.C. Rayner, G.J. Wright, A.F. Cowman, B. S. Crabb, Revealing the sequence and resulting cellular morphology of receptor-ligand interactions during *Plasmodium falciparum* invasion of erythrocytes, PLoS Pathog. 11 (2) (2015), https://doi.org/10.1371/journal.ppat.1004670 e1004670.
[4] A.L. Burns, M.G. Dans, J.M. Balbin, T.F. de Koning-Ward, P.R. Gilson, J.G. Beeson, M.J. Boyle, D.W. Wilson, Targeting malaria parasite invasion of red blood cells as antimalarial strategy, FEMS Microbiol. Rev. 43 (3) (2019) 223–238, https://doi.org/10.1093/femsre/fuz005.
[5] X. Gao, K. Gunalan, S.S.L. Yap, P.R. Preiser, Triggers of key calcium signals during erythrocyte invasion by *Plasmodium falciparum*, Nat. Commun. 4 (2013) 2862, https://doi.org/10.1038/ncomms3862.
[6] M. Brochet, O. Billker, Calcium signaling in malaria parasites, Mol. Microbiol. 100 (3) (2016) 397–408, https://doi.org/10.1111/mmi.13324.
[7] K. Leykauf, M. Treeck, P.R. Gilson, T. Nebl, T. Braulke, A.F. Cowman, T. W. Gilberger, B.S. Crabb, Protein kinase a dependent phosphorylation of apical membrane antigen 1 plays an important role in erythrocyte invasion by the malaria parasite, PLoS Pathog. 6 (6) (2010), e1000941, https://doi.org/10.1371/journal.ppat.1000941.

[8] B. Prinz, K.L. Harvey, L. Wilcke, U. Ruch, K. Engelberg, L. Biller, I. Lucet, S. Erkelenz, D. Heincke, T. Spielmann, C. Doerig, C. Kunick, B.S. Crabb, P.R. Gilson, T.W. Gilberger, Hierarchical phosphorylation of apical membrane antigen 1 is required for efficient red blood cell invasion by malaria parasites, Sci. Rep. 6 (2016) 34479, https://doi.org/10.1038/srep34479.

[9] D.A. Baker, L.G. Drought, C. Flueck, S.D. Nofal, A. Patel, M. Penzo, E.M. Walker, Cyclic nucleotide signaling in malaria parasites, Open Biol. 7 (12) (2017) 170213, https://doi.org/10.1098/rsob.170213.

[10] C. Syin, D. Parzy, F. Traincard, I. Boccaccio, M.B. Joshi, D.T. Lin, X.M. Yang, K. Assemat, C. Doerig, G. Langsley, The H89 cAMP-dependent protein kinase inhibitor blocks *Plasmodium falciparum* development in infected erythrocytes, Eur. J. Biochem. 268 (18) (2001) 4842–4849, https://doi.org/10.1046/j.1432-1327.2001.02403.x.

[11] A. Patel, A.J. Perrin, H.R. Flynn, C. Bisson, C. Withers-Martinez, M. Treeck, C. Flueck, G. Nicastro, S.R. Martin, A. Ramos, T.W. Gilberger, A.P. Snijders, M. J. Blackman, D.A. Baker, Cyclic AMP signaling controls key components of malaria parasite host cell invasion machinery, PLoS Biol. 7 (5) (2019), e3000264, https://doi.org/10.1371/journal.pbio.3000264.

[12] K. Yahata, M. Treeck, R. Culleton, T.W. Gilberger, O. Kaneko, Time-lapse imaging of red blood cell invasion by the rodent malaria parasite *Plasmodium yoelii*, PLoS One 7 (12) (2012), e50780, https://doi.org/10.1371/journal.pone.0050780.

[13] Y. Kegawa, M. Asada, T. Ishizaki, K. Yahata, O. Kaneko, Critical role of erythrocyte binding-like protein of the rodent malaria parasite *Plasmodium yoelii* to establish an irreversible connection with the erythrocyte during invasion, Parasitol. Int. 67 (6) (2018) 706–714, https://doi.org/10.1016/j.parint.2018.07.006.

[14] C.R. Collins, S. Das, E.H. Wong, N. Andenmatten, R. Stallmach, F. Hackett, J.-P. Herman, S. Muller, M. Meissner, M.J. Blackman, Robust inducible Cre recombinase activity in the human malaria parasite *Plasmodium falciparum* enables efficient gene deletion within a single asexual erythrocyte growth cycle, Mol. Microbiol. 88 (4) (2013) 687–701, https://doi.org/10.1111/mmi.12206.

[15] R.S. Kent, K.K. Modrzynska, R. Cameron, N. Philip, O. Billker, A.P. Waters, Inducible developmental reprogramming redefines commitment to sexual development in the malaria parasite *Plasmodium berghei*, Nat. Microbiol. 3 (11) (2018) 1206–1213, https://doi.org/10.1038/s41564-018-0223-6.

[16] T. Ishizaki, N. Chaiyawong, H. Hakimi, M. Asada, M. Tachibana, T. Ishino, K. Yahata, O. Kaneko, A novel *Plasmodium yoelii* pseudokinase, PypPK1, is involved in erythrocyte invasion and exflagellation center formation, Parasitol. Int. 76 (2020) 102056, https://doi.org/10.1016/j.parint.2020.102056.

[17] E. Knuepfer, M. Napiorkowska, C. van Ooij, A.A. Holder, Generating conditional gene knockouts in *Plasmodium* – a toolkit to produce stable DiCre recombinase-expressing parasite line using CRISPR/Cas9, Sci. Rep. 7 (1) (2017) 3881, https://doi.org/10.1038/s41598-017-03984-3.

[18] R.Y. Orr, N. Philip, A.P. Waters, Improved negative selection protocol for *Plasmodium berghei* in the rodent malaria model, Malar. J. 11 (2012) 103, https://doi.org/10.1186/1475-2875-11-103.

[19] H. Hakimi, T. Ishizaki, Y. Kegawa, O. Kaneko, S.I. Kawazu, M. Asada, Genome editing of *Babesia bovis* using CRISPR/Cas9 system, mSphere 4 (3) (2019), https://doi.org/10.1128/mSphere.00109-19 e00109-19.

[20] J.K. Mutungi, K. Yahata, M. Sakaguchi, O. Kaneko, Expression and localization of rhoptry neck protein 5 in merozoites and sporozoites of *Plasmodium yoelii*, Parasitol. Int. 63 (6) (2014) 794–801, https://doi.org/10.1016/j.parint.2014.07.013.

[21] W.S. Rasband, ImageJ, U.S. National Institutes of Health, Bethesda, Maryland, USA, 1997-2021. https://imagej.nih.gov/ij/.

[22] J.K. Mutungi, K. Yahata, M. Sakaguchi, O. Kaneko, Isolation of invasive *Plasmodium yoelii* merozoites with a long half-life to evaluate invasion dynamics and potential invasion inhibitors, Mol. Biochem. Parasitol. 204 (1) (2015) 26–33, https://doi.org/10.1016/j.molbiopara.2015.12.003.

[23] S.A. Ogun, R. Tewari, T.D. Otto, S.A. Howell, E. Knuepfer, D.A. Cunningham, Z. Xu, A. Pain, A.A. Holder, Targeted disruption of Py235ebp-1: invasion of erythrocytes by *Plasmodium yoelii* using an alternative Py235 erythrocyte binding protein, PLoS Pathog. 7 (2) (2011), e1001288, https://doi.org/10.1371/journal.ppat.1001288.

[24] H. Otsuki, O. Kaneko, A. Thongkukiatkul, M. Tachibana, H. Iriko, S. Takeo, T. Tsuboi, M. Torii, Single amino acid substitution in *Plasmodium yoelii* erythrocyte ligand determines its localization and controls parasite virulence, Proc. Natl. Acad. Sci. U. S. A. 106 (17) (2009) 7167–7172, https://doi.org/10.1073/pnas.0811313106.

[25] D.L. Narum, V. Nguyen, Y. Zhang, J. Glen, R.L. Shimp, L. Lambert, I.T. Ling, K. Reiter, S.A. Ogun, C. Long, A.A. Holder, R. Herrera, Identification and characterization of the *Plasmodium yoelii* PyP140/RON4 protein, an orthologue of *Toxoplasma gondii* RON4, whose cysteine-rich domain does not protect against lethal parasite challenge infection, Infect. Immun. 76 (11) (2008) 4876–4882, https://doi.org/10.1128/IAI.01717-07.

[26] O. Kaneko, T. Tsuboi, I.T. Ling, S. Howell, M. Shirano, M. Tachibana, Y.M. Cao, A. A. Holder, M. Torii, The high molecular mass rhoptry protein, RhopH1, is encoded by members of the *clag* multigene family in *Plasmodium falciparum* and *Plasmodium yoelii*, Mol. Biochem. Parasitol. 118 (2) (2001) 223–231, https://doi.org/10.1016/s0166-6851(01)00391-7.

[27] M.R. van Dijk, B.C.L. van Schaijk, S.M. Khan, M.W. van Dooren, J. Ramesar, S. Kaczanowski, G.-J. van Gemart, H. Kroeze, H.G. Stunnenberg, W.M. Eling, R. W. Sauerwein, A.P. Waters, C.J. Janse, Three members of the 6-cys protein family of *Plasmodium* play a role in gamete fertility, PLoS Pathog. 6 (4) (2010), https://doi.org/10.1371/journal.ppat.1000853 e1000853.

[28] M.-L. Wilde, T. Triglia, D. Marapana, J.K. Thompson, A.A. Kouzmitchev, H. E. Bullen, P.R. Gilson, A.F. Cowman, C.J. Tonkin, Protein kinase A is essential for invasion of *Plasmodium falciparum* into human erythrocytes, mBio 10 (5) (2019), https://doi.org/10.1128/mBio.01972-19 e01972-19.

[29] S. Absalon, K. Blomqvist, R.M. Rudlaff, T.J. DeLano, M.P. Pollastri, J.D. Dvorin, Calcium-dependent protein kinase 5 is required for release of egress-specific organelles in *Plasmodium falciparum*, mBio 9 (1) (2018), https://doi.org/10.1128/mBio.00130-18 e00130-18.

[30] K. Yahata, M.N. Hart, H. Davies, M. Asada, T.J. Templeton, M. Treeck, R.W. Moon, O. Kaneko, Gliding motility of *Plasmodium* merozoites, bioRxiv (2020), https://doi.org/10.1101/2020.05.01.072637, 2020.05.01.072637.

[31] P. Pino, S. Sebastian, E.A. Kim, E. Bush, M. Brochet, K. Volkmann, E. Kozlowski, M. Llinas, O. Billker, D. Soldati-Favre, A tetracycline-repressible transactivator system to study essential genes in malaria parasites, Cell Host Micobe 12 (6) (2012) 824–834, https://doi.org/10.1016/j.chom.2012.10.016.

[32] K.S. Harris, J.L. Casey, A.M. Coley, R. Masciantonio, J.K. Sabo, D.W. Keizer, E. F. Lee, A. McMahon, R.S. Norton, R.F. Anders, M. Foley, Binding hot spot for invasion inhibitory molecules on *Plasmodium falciparum* apical membrane antigen 1, Infect. Immun. 73 (10) (2005) 6981–6989, https://doi.org/10.1128/IAI.73.10.6981-6989.2005.

[33] M. Treeck, S. Zacheri, S. Herrmann, A. Cabrera, M. Kono, N.S. Struck, K. Engelberg, S. Haase, F. Frischknecht, K. Miura, T. Spielmann, T.W. Gilberger, Functional analysis of the leading malaria vaccine candidate AMA-1 reveals an essential role for the cytoplasmic domain in the invasion process, PLoS Pathog. 5 (3) (2009), e1000322, https://doi.org/10.1371/jopurnal.ppat.1000322.

[34] J. Cao, O. Kaneko, A. Thongkukiatkul, M. Tachibana, H. Otsuki, Q. Gao, T. Tsuboi, M. Torii, Rhoptry neck protein RON2 forms a complex with microneme protein AMA1 in *Plasmodium falciparum* merozoites, Parasitol. Int. 58 (1) (2009) 29–35, https://doi.org/10.1016/j.parint.2008.09.005.

[35] M. Lamarque, S. Besteiro, J. Papoin, M. Roques, B.V.L. Normand, J. Morlon-Guyot, J.-F. Dubremetz, S. Fauquenoy, S. Tomavo, B.W. Faber, C.H. Kocken, A.W. Thomas, M.J. Boulanger, G.A. Bentley, M. Lebrun, The RON2-AMA1 interaction is critical step in moving junction-dependent invasion by apicomplexan parasites, PLoS Pathog. 7 (2) (2011), e1001276, https://doi.org/10.1371/journal.ppat.1001276.

[36] P. Srinivasan, W.L. Beatty, A. Diouf, R. Herrera, X. Ambroggio, J.K. Moch, J. S. Tyler, D.L. Narum, S.K. Pierce, J.C. Boothyord, J.D. Haynes, L.H. Miller, Binding of *Plasmodium* merozoite proteins RON2 and AMA1 triggers commitment to invasion, Proc. Natl. Acad. Sci. U. S. A. 108 (32) (2011) 13275–13280, https://doi.org/10.1073/pnas.1110303108.